J. Phys. B: At. Mol. Opt. Phys. **41** (2008) 045302 (12pp) doi:10.1088/0953-4075/41/4/045302

Numerical study of one-dimensional and interacting Bose–Einstein condensates in a random potential

Eric Akkermans[1], **Sankalpa Ghosh**[1,2] **and Ziad H Musslimani**[3]

[1] Department of Physics, Technion Israel Institute of Technology, 32000 Haifa, Israel
[2] Physics Department, Indian Institute of Technology Delhi, New Delhi 110 016, India
[3] Department of Mathematics, Florida State University, Tallahassee, FL 32306-451, USA

Received 12 October 2007, in final form 19 December 2007
Published 11 February 2008
Online at stacks.iop.org/JPhysB/41/045302

Abstract

We present a detailed numerical study of the effect of a disordered potential on a confined one-dimensional Bose–Einstein condensate, in the framework of a mean-field description, using a highly efficient and fast converging numerical scheme. For repulsive interactions, we consider the Thomas–Fermi and Gaussian limits and for attractive interactions the behaviour of soliton solutions. We find that the average spatial extension of the stationary density profile decreases with an increasing disorder strength both for repulsive and attractive interactions among bosons. In the Thomas–Fermi limit, a strong localization of the bosons is obtained in momentum space around the state $k = 0$. The time-dependent density differs considerably in the cases we have considered. For attractive and disordered Bose–Einstein condensates, we show evidence of a bright soliton with an overall unchanged shape, but a disorder-dependent width. For weak disorder, the soliton is delocalized and for stronger disorder, it bounces back and forth between high potential barriers.

(Some figures in this article are in colour only in the electronic version)

1. Introduction

The spatial behaviour of a wave submitted to a strong enough random potential remains one of the major and still unsolved issues in physics. It is a ubiquitous problem that shows up in almost all fields ranging from astrophysics to atomic physics. The interference induced spatial localization of a wave due to random multiple scattering has been predicted and named after Anderson [1]. The Anderson localization problem despite its relatively easy formulation has not yet been solved analytically and still raises a lot of interest. Strong Anderson localization of waves has been observed in various systems of low spatial dimensionality where the effect of disorder is expected to be the strongest [2–4]. Above two dimensions, a phase transition is expected to take place between a delocalized phase that corresponds to spatially extended solutions of the wave equation and a localized phase that corresponds to spatially localized solutions. The description of this transition is mainly based on an elegant scaling formulation proposed by Anderson and coworkers [5]. Due to its indisputable importance, the localization of light is a hotly debated but still unsolved problem [6–9]. The weak localization regime, a precursor of Anderson localization for weak disorder, has been studied in detail both theoretically and experimentally for a large variety of waves and types of disorder [10–13].

In contrast, relatively little attention has been paid to the extension of Anderson localization to a nonlinear medium. Though analytical [14–16] as well as numerical work has been done to address this issue, no clear-cut answers have been obtained to ascertain how localization is affected by the presence of a nonlinear term in a Schrödinger-type wave equation. It is the purpose of this paper to address this issue in the context of the behaviour of a one-dimensional Bose–Einstein condensate (BEC) in the presence of a disordered optical potential, since it has raised recently a great deal of interest [17–30]. Transport of a magnetically trapped BEC above a corrugated microchip has been theoretically studied recently [31]. The possibility of tuning random on-site interaction has also been considered [32]. Using Feshbach resonances, it is possible to switch off the interaction

among bosons which will then be allowed to propagate through a set of static impurities created by other species of atom. This may lead to an experimental realization of the Anderson localization transition. The corresponding theoretical model has been proposed and analysed [26, 27] for one-dimensional systems, i.e. in the absence of transition. The other issue is to understand the interplay of interaction induced nonlinearity and disorder on the Bose–Einstein condensate. One-dimensional systems are especially interesting since the effect of disorder is the strongest and such systems are experimentally realizable. Experiments in this direction have been performed recently [17, 18, 20] which show a suppression of the expansion of the BEC cloud once it is released from the trap.

In this paper we present a numerical study of the effect of a disordered potential on one-dimensional condensates with either attractive or repulsive interaction in the framework of the mean-field approximation and compare between these two cases. We use a highly efficient and fast converging numerical scheme based on spectral renormalization. It is particularly suitable for systems where both randomness and nonlinearity are present. Another useful feature of our model of disorder is that both its strength and its harmonic content can be independently varied.

Studies of the propagation of a quasi-one-dimensional BEC in a disordered potential have been carried out mostly in the repulsive Thomas–Fermi limit [17, 18, 20, 22, 30]. We also consider this limit and find numerical evidence that the suppression of the BEC expansion after the release from the trap is due to localization in momentum space around the state $k = 0$, which becomes stronger for an increasing strength of disorder. This suggests that the momentum spectroscopy of disordered quasi-one-dimensional BEC may provide important information about its transport properties. In addition, we consider the Gaussian limit of a strong confinement and the bright soliton solution for an attractive interaction.

The interplay between these different types of interaction and disorder leads to different kinds of stationary and time-dependent behaviour of the density profile. We consider three regimes that cover both the repulsive and attractive interaction and where the system can indeed be well described within the mean-field approximation. It is given by the Gross–Pitaevskii equation with modified coupling constant [34] and it reduces to a nonlinear Schrödinger equation whose solutions in the absence of disorder have been thoroughly studied [36, 38–40]. We employ a recently developed numerical scheme based on a rapidly converging spectral method [42–45] to study stationary solutions of this nonlinear Schrödinger equation in the presence of a disordered potential. Then, we look at the time evolution of the stationary profile after switching off the trap potential. Subsequently, we analyse our solutions and compare them to those obtained in the absence of disorder.

The organization of the paper is as follows. In section 2, we briefly review the stationary density profiles of an effectively one-dimensional BEC in the absence of disorder and in the mean-field regime. Then, in section 3, we describe our numerical scheme and define our model of disorder. In section 4, we present our numerical results for the Thomas–Fermi limit. In section 4.1 we compare them to recent works [17, 18, 20, 22, 30, 31]. In section 5, the effect of disorder in the confinement-dominated Gaussian regime is discussed. Both sections pertain to the case of repulsive interaction among bosons. In section 6, we show the existence, for an attractive effective interaction, of a stable bright solitonic condensate in the presence of disorder and we study its dynamics. In the last section we summarize and present the general conclusions derived from our results.

2. Stationary solutions in the absence of disorder

2.1. One-dimensional repulsive Bose–Einstein condensate in a trap

We review briefly the mean-field description of a quasi-one-dimensional Bose gas with short-range repulsive interaction, in a cylindrical harmonic trap along the z-axis, and in the absence of disorder. Details are given in [35, 36]. The Gross–Pitaevskii equation provides a mean-field description of the three-dimensional interacting gas and it is given by

$$\mathrm{i}\hbar\frac{\partial\Psi}{\partial t} = -\frac{\hbar^2}{2m}\nabla^2\Psi + \frac{1}{2}\left(m\omega_z^2 z^2 + m\omega_\perp^2(x^2+y^2)\right)\Psi + \frac{4\pi a\hbar^2}{m}|\Psi|^2\Psi \tag{1}$$

where ω_z and $\omega_\perp$ are respectively the harmonic trap frequencies along the z-axis and the radial direction; $a_z = \sqrt{\frac{\hbar}{m\omega_z}}$ and $a_\perp = \sqrt{\frac{\hbar}{m\omega_\perp}}$ are the corresponding harmonic oscillator length scales. The interaction is characterized by the s-wave scattering length a that is positive for a repulsive interaction. For tight trapping conditions ($\omega_z \ll \omega_\perp$), all atoms are in the ground state of the harmonic trap in the radial direction and the condensate is effectively one dimensional. Nevertheless, for $a_\perp > a$, the effective coupling constant along the z-direction is still characterized by a and it is given by $g_{1\mathrm{d}} = 2a\hbar\omega_\perp$ [34]. The corresponding mean-field behaviour is governed by the Gross–Pitaevskii equation,

$$\mathrm{i}\hbar\frac{\partial\Psi}{\partial t} = -\frac{\hbar^2}{2m}\frac{\partial^2\Psi}{\partial z^2} + \frac{1}{2}m\omega_z^2 z^2\Psi + g_{1\mathrm{d}}|\Psi|^2\Psi, \tag{2}$$

where Ψ is the condensate wavefunction along the z-axis. We look for stationary solutions of the form $\Psi(z,t) = \phi(z)\exp\left(-\mathrm{i}\frac{\tilde{\mu}}{\hbar}t\right)$ where $\tilde{\mu}$ is the chemical potential. The corresponding one-dimensional density is $\rho_{1\mathrm{d}} = |\phi(z)|^2$. The interaction strength may be expressed in terms of the dimensionless coupling constant γ,

$$\gamma = \frac{mg_{1\mathrm{d}}}{\hbar^2\rho_{1\mathrm{d}}}, \tag{3}$$

which is the ratio of the mean-field interaction energy density to the kinetic energy density. For $\gamma \ll 1$, the gas is weakly interacting and, in contrast to higher space dimensionalities, in one dimension the gas can be made strongly interacting by lowering its density. For larger values of the interaction strength γ, the Gross–Pitaevskii equation (2) does no longer provide a correct description, the gas enters into the Tonks–Girardeau regime [37] and behaves like free fermions.

Starting from (2), a dimensionless form can be achieved that is given by

$$\mathrm{i}\partial_t \Psi + \partial_z^2 \Psi - z^2 \Psi - 2\alpha_{1\mathrm{d}} |\Psi|^2 \Psi = 0, \tag{4}$$

where the use has been made of rescaled length and time, $z \to \frac{z}{a_z}$, $t \to \frac{\omega_z}{2} t$ and $\Psi \to \sqrt{a_z}\Psi$. The dimensionless parameter $\alpha_{1\mathrm{d}}$, or equivalently the coherence length ξ, is defined by

$$\alpha_{1\mathrm{d}} = \frac{2aa_z}{a_\perp^2} = \frac{1}{2\xi^2}, \tag{5}$$

and it accounts for both interaction and confinement. By rescaling the chemical potential, $\mu \to \frac{2\tilde{\mu}}{\hbar\omega_z}$, we obtain for the time-independent Gross–Pitaevskii equation the expression

$$\mu\phi + \partial_z^2 \phi - z^2 \phi - 2\alpha_{1\mathrm{d}} |\phi|^2 \phi = 0. \tag{6}$$

Henceforth we shall express our results in terms of these dimensionless quantities unless otherwise specified. We mention now two limiting regimes of interest that can be described by equation (6).

2.1.1. Thomas–Fermi limit. For a chemical potential $\tilde{\mu}$ larger than the level spacing, namely for $\tilde{\mu} \gg \hbar\omega_z$ (i.e. in dimensionless units $\mu \gg 1$), the gas is in the Thomas–Fermi regime. Thus the kinetic energy term becomes negligible. We denote by ρ_{TF} and μ_{TF} the corresponding condensate density and chemical potential. We have

$$\rho_{\mathrm{TF}} = \frac{\mu_{\mathrm{TF}} - z^2}{2\alpha_{1\mathrm{d}}} \Theta(\mu_{\mathrm{TF}} - z^2). \tag{7}$$

The number of bosons is given by $N = \int_{-L_{\mathrm{TF}}}^{L_{\mathrm{TF}}} \mathrm{d}z \rho_{\mathrm{TF}}$, where $L_{\mathrm{TF}} = \sqrt{\mu_{\mathrm{TF}}}$ is the Thomas–Fermi length. Eliminating L_{TF}, we obtain

$$\mu_{\mathrm{TF}} = \left(\frac{3N\alpha_{1\mathrm{d}}}{8}\right)^{2/3}. \tag{8}$$

2.1.2. Gaussian limit. The opposite limit $\tilde{\mu} \ll \hbar\omega_z$ corresponds to a regime where the single-particle energy spacing is larger than the interaction energy so that the gas behaves like N bosons in a harmonic trap potential. Thus, we have an ideal gas condensate with a Gaussian density profile.

As we shall see later, the effect of a disordered potential on the condensate dynamics for both limiting cases is significantly different.

2.2. One-dimensional attractive Bose–Einstein condensate

We also consider the case where the s-wave scattering length a is negative. The effective interaction among bosons is thus attractive. This situation can also be described by means of equations (2)–(4). In the absence of confinement and for $\alpha_{1\mathrm{d}} = -1$ [40], equation (4), provided the total number of particles $N = \int \mathrm{d}z |\Psi|^2$ is less than a critical number N_c beyond which the condensate collapses, admits a moving bright soliton solution of the form

$$\Psi(z,t) = \sqrt{\mu} \frac{\exp\left(\mathrm{i}\left(\frac{V_s}{2} z + \left(\mu - \frac{V_s^2}{4}\right)t + \phi_0\right)\right)}{\cosh(\sqrt{\mu}(z - V_s t - z_0))} \tag{9}$$

where V_s and $\mu > 0$ are respectively the velocity and the chemical potential of the soliton and (z_0, ϕ_0) refer to the translational and global phase invariance of equation (4). In particular, if $V_s = 0$ and choosing for simplicity the gauge $z_0 = \phi_0 = 0$, then $\Psi(z,t) = \phi(z)\exp(\mathrm{i}\mu t)$ with

$$\phi(z) = \sqrt{\mu}\,\mathrm{sech}(\sqrt{\mu} z), \tag{10}$$

which satisfies the time-independent nonlinear Schrödinger equation

$$-\mu\phi(z) + \partial_z^2 \phi(z) + 2|\phi|^2 \phi = 0. \tag{11}$$

The chemical potential μ is proportional to the square of the inverse width of the soliton. Such a soliton has been experimentally observed [38] and theoretically studied [39] for cold atomic gases.

3. Numerical method for disorder and nonlinearity

3.1. Spectral method

We start by considering the dimensionless time-independent Gross–Pitaevskii equation

$$\mu\phi + \partial_z^2 \phi - z^2 \phi(z) - V_d(z)\phi - 2\alpha_{1\mathrm{d}} |\phi|^2 \phi = 0, \tag{12}$$

in the presence of a disorder potential $V_d(z)$. Upon discretization, this potential is defined at each site of a lattice and it is given by the product of a constant strength V_m times a random number ω which is uniformly distributed between 0 and 1. This model slightly differs from the one usually used, where the disorder potential has a Gaussian distribution [41]. However, Anderson localization does not depend on such characteristics of the disorder potential. Using a Gaussian approximation with mean σ (the lattice spacing), the disorder potential can be written as a continuous function

$$V_d(z,\omega) = \omega V(z) \tag{13}$$

with

$$V(z - z') = \lim_{\sigma \to 0} V_m \exp\left(-\frac{(z' - z)^2}{\sigma^2}\right). \tag{14}$$

A disorder potential generated in this way varies rapidly over a length scale of the order of a lattice spacing. We wish however to use a smoother potential more appropriate for the description of typical disorders generated in experiments [17, 20]. To that purpose, we consider the discrete random variable ω defined at each lattice site and we remove from its Fourier spectrum all wavenumbers that are above a given cutoff $k_c = 2\pi/\lambda_c$. The inverse Fourier transform $\omega(\lambda_c) = \omega^c$ provides a random potential that varies on length scales larger than or equal to λ_c and which can be formally written as

$$V^c(z) = V_m \int \mathrm{d}k\, \mathrm{e}^{\mathrm{i}kz} \left[\mathrm{e}^{-\left(\frac{k}{k_c}\right)^M} \int \mathrm{d}\zeta\, \omega(\zeta)\, \mathrm{e}^{-\mathrm{i}k\zeta}\right], \tag{15}$$

where M is a large enough number. The new random variable $\omega^c(\lambda_c, z)$ thus generated is different from ω. While the average value of ω is, by definition, equal to 1/2, we obtain, for example, that for $k_c = 6$, the average value of ω^c is about 2×10^{-2}. Typical examples of such slowly varying potentials obtained by changing λ_c are given in figures 8(a), (c) and (e). The disorder potential $V^c = V_m \omega^c(\lambda_c, z)$ that we consider is

thus characterized by two quantities: its strength V_m and the scale λ_c of its spatial variations. Equation (12) rewrites

$$\mu\phi_\omega + \partial_z^2\phi_\omega - z^2\phi_\omega - V_m\omega^c(\lambda_c, z)\phi_\omega - 2\alpha_{1d}|\phi_\omega|^2\phi_\omega = 0. \tag{16}$$

The local density for a given realization of disorder is $\rho_\omega(z) = |\phi_\omega(z)|^2$ and the number N of bosons is determined by the condition $N = \int \mathrm{d}z\rho_\omega(z)$. By direct inspection of the different terms that appear in equation (16), we see that disorder effects are obtained either by comparing them to interactions, i.e., by comparing the disorder length scale λ_c to the coherence length ξ defined in (5). If the ratio λ_c/ξ is small, disorder is strongly varying spatially and its effect overcomes that of interactions. We also compare the effective disorder strength $V_m\omega^c$ to the chemical potential μ. This can be achieved by defining the local dimensionless random variable

$$s = \frac{V_m}{\mu}\omega^c. \tag{17}$$

We will consider its average over configurations denoted by $\langle s\rangle$. The parameter s allows us to compare the chemical potential and amplitude of disorder potential barriers. This parameter, as we shall see, plays also an important role in the study of the time evolution of the density once the trapping potential is released. It is a measure of the spatial extension of the cloud as a function of time. Finally, we consider boundary conditions for equation (16) obtained by demanding that for a given realization of disorder, $\phi_\omega(z)$ vanishes for $|z| \longrightarrow +\infty$.

We now turn to the description of the numerical method used to solve equation (16). The fact that it is random makes it very challenging for conventional numerical schemes to be implemented. The numerical scheme we use here is based on the spectral renormalization method that has been recently proposed by Ablowitz and Musslimani [45] (see also [43, 44]) as a generalization of the Petviashvili method [42]. Spectral renormalization is particularly suitable for this type of problems for its ease to handle randomness. Consider, for a fixed realization, the Fourier transform

$$\hat\phi_\omega(k) = \mathcal{F}[\phi_\omega(z)] = \int \mathrm{d}z\phi_\omega(z)\,\mathrm{e}^{-\mathrm{i}kz}. \tag{18}$$

By Fourier transforming equation (16) we obtain

$$\hat\phi_\omega(k) = \frac{2\alpha_{1d}\mathcal{F}[|\phi_\omega|^2\phi_\omega] + \mathcal{F}[z^2\phi_\omega(z)] + \mathcal{F}[V^c(z,\omega)\phi_\omega]}{\mu - k^2}. \tag{19}$$

Generally, the solution of this equation is obtained by a relaxation method or a successive approximation technique where a given initial guess is iterated until convergence is achieved. However, this relaxation process is unlikely to converge. To prevent this problem, we introduce a new field variable $\psi_\omega(z)$ using a scaling parameter p_ω,

$$\phi_\omega(z) = p_\omega\psi_\omega(z), \qquad \hat\phi_\omega(k) = p_\omega\hat\psi_\omega(k). \tag{20}$$

Substituting into equation (19) and adding and subtracting the term $r\hat\phi_\omega(k)$ (with $r > 0$) to avoid division by zero, we obtain the following scheme,

$$\hat\psi_\omega^{(m+1)}(k) = \left(\frac{r+\mu}{r+k^2}\right)\hat\psi_\omega^{(m)} - \frac{\mathcal{F}\left[z^2\psi_\omega^{(m)}\right]}{r+k^2} - \frac{\mathcal{F}\left[V^c(z,\omega)\psi_\omega^{(m)}\right]}{r+k^2} - 2\alpha_{1d}\left|p_\omega^{(m)}\right|^2\frac{\mathcal{F}\left[\left|\psi_\omega^{(m)}\right|^2\psi_\omega^{(m)}\right]}{r+k^2}, \tag{21}$$

where $p_\omega^{(m)}$ are given by the following consistency condition,

$$\left|p_\omega^{(m)}\right|^2 = \frac{\langle\hat\psi_\omega^{(m)}, (\mu-k^2)\hat\psi_\omega^{(m)} - \mathcal{F}\left[z^2\psi_\omega^{(m)}\right] - \mathcal{F}\left[V^c\psi_\omega^{(m)}\right]\rangle}{\langle\hat\psi_\omega^{(m)}, \mathcal{F}\left[\left|\psi_\omega^{(m)}\right|^2\psi_\omega^{(m)}\right]\rangle}, \tag{22}$$

where the inner product in the Fourier space is defined by

$$\langle\hat f, \hat g\rangle = \int \hat f\hat g\,\mathrm{d}k.$$

We have checked that the above method generally converges much faster in comparison to the method like imaginary time propagation. Also the condition and dependence on the initial ansatz solution is much less forceful than in comparable methods, such as Newton's search algorithm.

3.2. Time-dependent evolution

To describe the time evolution of the stationary solutions, we use a time splitting Fourier spectral method that has been described in detail elsewhere [46]. We describe it briefly with a comment on its limitation.

After switching off the trap, the time evolution is governed by the equation

$$\mathrm{i}\partial_t\Psi_\omega(z,t) = -\partial_z^2\Psi_\omega(z,t) + V_m\omega^c(\lambda_c, z)\Psi_\omega(z,t) + 2\alpha_{1d}|\Psi_\omega(z,t)|^2\Psi_\omega(z,t), \tag{23}$$

with $\Psi_\omega(z,0) = \phi_\omega(z)$. Equation (23) is solved in two distinct steps. We solve first

$$\mathrm{i}\partial_t\Psi_\omega(z,t) = -\partial_z^2\Psi_\omega(z,t), \tag{24}$$

for a time step of length Δt and then

$$\mathrm{i}\partial_t\Psi_\omega(z,t) = V_m\omega^c(\lambda_c, z)\Psi_\omega(z,t) + 2\alpha_{1d}|\Psi_\omega(z,t)|^2\Psi_\omega(z,t), \tag{25}$$

for the same time step. The first of these two equations, (24), is discretized in space by the Fourier spectral method and time integrated. The solution is then used as the initial condition for the second equation (25). The commutator between the two parts of the Hamiltonian that appears on the right-hand side of (24) and (25) is disregarded in this process. The resulting error is significant if this commutator is large compared to other terms in the equation. This is the case if the disordered potential strongly fluctuates (which is not considered in the present numerical work). Note that, by definition, this method ensures the conservation of the total number of particles.

4. Thomas–Fermi limit

4.1. Stationary solutions

Stationary solutions to the Gross–Pitaevskii equation (12) in the Thomas–Fermi limit are obtained by iterating equations (21) and (22). Then, we compare these solutions with those obtained by directly considering the Thomas–Fermi approximation in the presence of disorder. This comparison is displayed in figure 1.

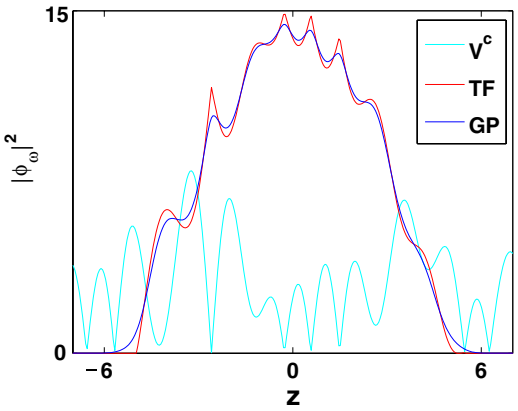

Figure 1. Behaviour of the condensate density $|\phi_\omega|^2$ obtained from the Thomas–Fermi approximation and from the Gross–Pitaevskii equation for a spatially rapidly varying disorder such that $\lambda_c \approx 2\xi$. The average disorder is kept much below the chemical potential ($\mu = 30$), so that $\langle s \rangle \ll 1$. We have taken $\alpha_{1d} = 1$ and a number N of bosons equal to 80.

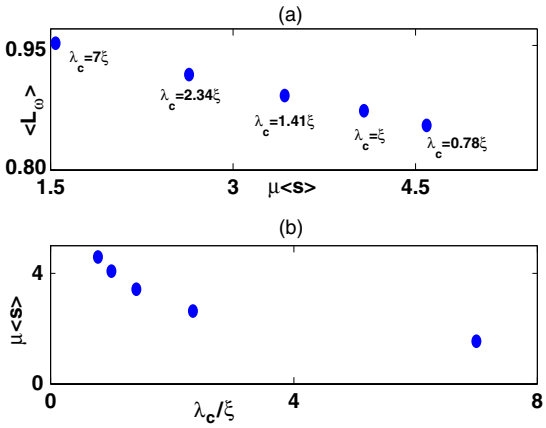

Figure 2. (a) Plot of the width $\langle L_\omega \rangle$ averaged over disorder, as a function of the average strength $\mu\langle s \rangle$. $\langle L_\omega \rangle$ is expressed in units of the corresponding extension in the absence of disorder. For a given value of λ_c, we average over 200 realizations of the disordered potential. The quantity $\langle s \rangle$ defined through equation (17) is calculated by averaging over these 200 configurations for each λ_c. The behaviour of $\mu\langle s \rangle$ as a function of $\frac{\lambda_c}{\xi}$ has been plotted in part (b). Such calculations have been done for five different values of λ_c, the last one being less than the coherence length ξ for which the validity of the mean-field theory is questionable. We have taken $\mu = 30$ and $\alpha_{1d} = 1$. (b) The plot showing the change of $\mu\langle s \rangle$ as the cut-off λ_c changes for the values used in the part (a).

Generalizing the Thomas–Fermi approximation (7) so as to include the disorder V^c, we obtain for the corresponding density the expression

$$\rho_{TF}(z) = \frac{\mu - z^2 - V^c}{2\alpha_{1d}}, \qquad \mu \geqslant z^2 + V^c = 0,$$
$$\mu < z^2 + V^c. \tag{26}$$

The density is thus expected to present local maxima and minima that follow those of the disordered potential.

While the typical number of speckles of the disorder potential used experimentally [17, 20–22] varies widely between 6 (LENS [17]) and 40–50 (Orsay [20]), the speckle size, in all the experiments, is much larger than ξ and much smaller than the Thomas–Fermi size of the condensate. To account for this experimental situation, we consider in figure 1 a strong disorder that fluctuates on a length scale λ_c comparable to ξ, but much smaller than the size of the condensate, thus leading to several local minima and maxima of the disordered potential within the size of the cloud.

We observe that the deviations from the Thomas–Fermi solution become larger as λ_c decreases, i.e., for larger spatial variations of disorder. This behaviour can be understood by considering the following expression for the density ρ_ω:

$$\rho_\omega = \frac{(\mu - z^2 - V^c(z))}{2\alpha_{1d}} + \xi^2 \left(\frac{\partial_z^2 \phi}{\phi}\right)$$
$$= \rho_{TF} + \xi^2 \left(\frac{\partial_z^2 \phi}{\phi}\right) \tag{27}$$

which follows straightforwardly from equation (16). In this expression, the second term on the rhs, also known as the quantum pressure term is a correction to the Thomas–Fermi density whose origin is the zero point motion of the bosons in the condensate. This correction is proportional to the ratio $(\xi/\lambda_c)^2$. It becomes larger for a decreasing λ_c, namely for a relatively larger effect of interactions driven by ξ. Thus a stronger disorder introduces more appreciable zero point motion of the bosons so as to reduce the interaction energy cost. In other words, the behaviour of the static Thomas–Fermi condensate in a random potential is such that the disorder potential becomes smoothened by the repulsive interaction [22, 33, 47]. In a recent work [47], such smoothening of disordered potential in the presence of an interaction term has been analysed perturbatively using a parameter essentially similar to $\left(\frac{\xi}{\lambda_c}\right)^2$. It is thus interesting to compare figure 2 in [47] with our figure 1, but after noticing some important differences between the models of disorder used in these two works. In [47], the disorder potential is either positive or negative with zero average, whereas in our case it is strictly positive and thus corresponds to potential barrier only and not potential wells. Moreover, quantum-mechanical bound states formed in potential wells contribute to the set of basis states, whereas in the present case, that possibility does not exist. The parameter σ_R that determines the average speckle size in that work, is different from λ_c which appears to generalize it [47] (see footnote 6 of [47]) for a random potential.

Another feature of disorder is the spatial extension of the cloud defined, for a given disorder configuration, by

$$L_\omega = \sqrt{\overline{z^2} - \overline{z}^2} \tag{28}$$

where we have characterized the spatial distribution of the cloud by its moments,

$$\overline{z^n} = \frac{\int \mathrm{d}z z^n \rho_\omega(z)}{\int \mathrm{d}z \rho_\omega(z)}. \tag{29}$$

In figure 2, we have plotted the configuration average $\langle L_\omega \rangle$ of the spatial extension as a function of the average strength $\mu\langle s \rangle$ (see equation (17)). The average spatial extension of the cloud in the Thomas–Fermi limit is a decreasing function of

the ratio λ_c/ξ, i.e., it decreases when interactions are getting larger than the spatial variation of disorder. We shall see that this behaviour holds also beyond the Thomas–Fermi approximation. In figure 2(b), we show how $\mu\langle s\rangle$ varies with λ_c.

The evolution of the disordered ground state has also been studied as a function of the interaction strength [22, 48].

4.2. Time evolution

We now study the time evolution of the previous stationary solutions while switching off the trapping potential, but keeping the disordered potential. The problem has been studied experimentally in [18, 20, 21] and theoretically in [18, 30, 49]. In the experiments [19, 22], the BEC was prepared within the trapping and random potentials, but its expansion has been studied while switching off both of them. This led to the observation of sharp fringes in the resulting density due to interference between different parts of the condensate. These conditions differ from the case we consider here.

We recall that our disorder is characterized by its strength s in units of the chemical potential μ and by the length scale λ_c of its spatial variations. The latter quantity is analogous to the disorder correlation length defined in [20]. It is important to stress that in the Thomas–Fermi regime, the time evolution is very sensitive to the existence of potential barriers of height larger than the chemical potential μ. If such a barrier exists, say at a point z_0, then we observe that the density $\rho_\omega(z)$ vanishes for $z \geqslant z_0$ at any subsequent times so that the cloud becomes spatially localized. Then, the average parameter $\langle s\rangle$ is no longer relevant since it may be smaller than unity although some barriers may be larger than μ. We thus need to characterize the disorder by means of higher moments. For a smooth enough probability distribution of the random variable $V_m\omega^c$, which is the case we consider, it is enough to consider the variance $\delta\omega^c$ defined by $\delta\omega^c = (\langle(\omega^c)^2\rangle - \langle\omega^c\rangle^2)^{1/2}$ and the parameter

$$\delta s = \frac{V_m}{\mu}\delta\omega^c \tag{30}$$

which sets the width of the distribution of potential barriers. In some of the cases we consider, the peak height of the disordered potential is twice as high as $V_m\delta_{\omega_c}$. A specific feature of the one-dimensional disorder is that it is always very strong in contrast to higher dimensional systems for which the cloud may always find a way to avoid large potential barriers thus making effects of disorder comparatively weaker. We have studied numerically the density profile $\rho_\omega(T)$ after a time T for different spatial variations of the disordered potential. A first general observation is that for small values of λ_c, i.e. for strong spatial fluctuations, the spatial expansion of the cloud is inhibited, and the cloud remains localized in finite regions that depend on the local landscape of the disordered potential. In figure 3 we present the time evolution of the density at the centre (high density) and on the edges (low density) [20, 49, 51].

After the trap potential is released, the density peak at the centre, which corresponds to the highest value of the stationary density, gets lowered at an initial stage of the expansion. The interaction energy remains larger than the kinetic energy so that the density profile near the centre still follows the Thomas–Fermi shape, but with a reduced chemical potential. The spatial variation of density fluctuations corresponds approximately to that of the disordered potential (of the order of λ_c). At the edges of the cloud, the density is lower so that the kinetic energy term takes over the interaction term and it is almost equal to the chemical potential μ of the condensate at $t = 0$. Thus, the characteristic scale of spatial variations of density fluctuations at the edges of the cloud is the coherence length ξ which is smaller than λ_c. This is displayed in figure 3 which depicts the time evolution at the centre ((a) and (b)) and at the edge ((c) and (d)). Particularly the features of figures 3(a) and (b) which correspond to stronger but smoother disorder, are in broad agreement with the result demonstrated in figure 8 of [21].

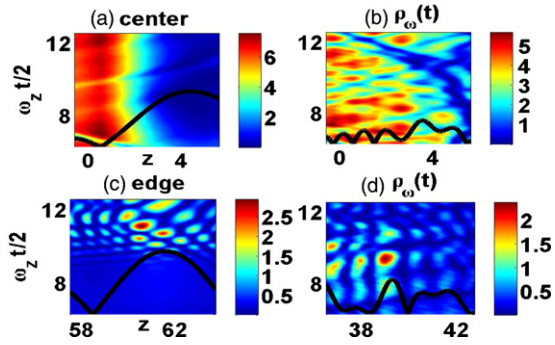

Figure 3. (a) and (c) Time evolution of the density at the centre and the edge for a strong disorder ($\langle s\rangle = 0.23$, $\delta s = 0.185$ and $\lambda_c = 12\xi$); (b) and (d) time evolution of the density at the centre and the edge for a disorder characterized by $\langle s\rangle = 0.095$, $\delta s = 0.076$, $\lambda_c = 2\xi$, $\mu = 30$ and $\alpha_{1d} = 1$ for all figures. The horizontal and vertical axes are the same for all plots and are shown in alternative pair of figures. The black line in each figure represents the disordered potential which is rescaled and its origin shifted by the same amount in all figures.

In figure 3(a), we show that after a time T, the centre of the cloud follows the potential landscape and varies on a larger length scale than the edge of the cloud. The other limit, $\lambda_c \simeq \xi$, shown in figures 3(b) and (d), displays relatively less difference between spatial variations of density fluctuations at the centre and at the edges of the cloud.

Figure 3 also describes how the matter wave behaves close to a single potential barrier placed either at the centre or at the edge of the cloud. In figures 3(a) and (b), the central cloud becomes localized due to the presence of a potential barrier. The density modulation is driven by the local potential landscape, rather than by any interference effect. It has been pointed out in [18, 30] that the height of a single defect should vary like the energy E of the incoming wavepacket over a distance short compared to its de Broglie wavelength in order to allow for quantum effects to dominate and eventually lead to Anderson localization. The potential used in our computation does not satisfy this criterion. To fulfil it, one needs a disorder with higher δs and lower λ_c. However under such conditions, the mean-field Gross–Pitaevskii approximation is questionable

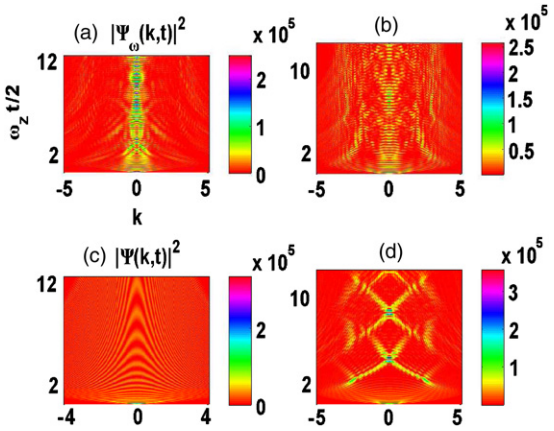

Figure 4. Evolution of the density in the k-space. Horizontal and vertical axis labels are identical for all the plots and are shown in (a). Part (a) corresponds to a strong disorder as defined in figure 3(c). (b) Weaker disorder fluctuating on a smaller length scale as defined in figure 3(b). (c) No disorder and (d) optical lattice: $(\langle s\rangle + \delta s)\sin\frac{2\pi z}{\lambda_c}$. The values of $\langle s\rangle$, δs and λ_c are those used in figure 3(c).

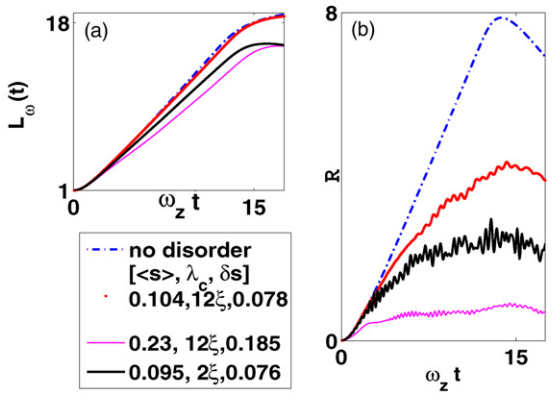

Figure 5. (a) Time evolution of the spatial extension $L_\omega(t)$ of the cloud as defined in (28) for a given configuration of the disordered potential but for different strengths V_m and length scales λ_c. $\langle s\rangle$, λ_c and δs are indicated against each plot. $L_\omega(t)$ is expressed in units of its value at $t = 0$. (b) Corresponding time evolution of the ratio $\mathcal{R}$ defined in (31).

and the use of the discrete nonlinear Schrödinger equation will be more appropriate.

We have studied in figure 4 the time evolution of the cloud density in momentum space and compare it to the cases without disorder and in the presence of an optical lattice. Figure 4(a) shows a strong localization in k-space for high values of δs. This is to be compared to the case of figure 4(d) (optical lattice). This strong localization occurs around the $k = 0$ state. On the other hand when disorder fluctuates on a shorter scale λ_c (with a smaller δs), a significant fraction of the density still occupies higher momentum states and the corresponding localization in momentum space is less pronounced. Thus, a measurement of the momentum spectrum [50] of a quasi-one-dimensional BEC in a disordered waveguide can shed light on the nature of localization of the cloud. It has been shown [49] that in the low-density tail of the expanding BEC cloud, each Fourier component having a low enough momentum becomes exponentially localized with a momentum-dependent localization length due to destructive interference. This signals Anderson localization. Such a behaviour shows up also for a two-dimensional condensate [51] and two distinct time scales can be identified over which the expansion of the cloud takes place, the first stage being dominated by nonlinearity and the second by disorder and thus more likely to show Anderson localization. In a recent experiment [52], an expanding highly elongated BEC has been imaged and reproducible interference fringes have been observed before the BEC gets fragmented into phase-incoherent pieces. However this interference pattern has been attributed to the overlap of different pieces of the expanding BEC with distinct velocities and not to multiple scattering and Anderson localization.

In the above discussion we have only considered the time evolution of the mean-field ground state. Small fluctuations around the mean-field solution and Anderson localization of Bogoliubov quasi-particles have been considered in detail by the Orsay group [53].

After studying the time evolution of the density, we consider other properties of the cloud that characterize the suppression of its spatial expansion. In figure 5(a), the spatial extension L_ω defined in (28) is plotted as a function of the dimensionless time $\omega_z t$. We observe that $L_\omega(t)$ saturates to a value which depends on the average strength $\langle s\rangle$ of the disorder in qualitative agreement with the experimental findings [21] and others.

In order to characterize this saturation, we define the ratio, denoted by $\mathcal{R}$, between the average kinetic and interaction energies of the cloud by

$$\mathcal{R} = 2\xi^2 \frac{\int \mathrm{d}z \left(\frac{\partial \phi_\omega}{\partial z}\right)^2}{\int \mathrm{d}z |\phi_\omega|^4}. \tag{31}$$

In the stationary Thomas–Fermi approximation, the kinetic energy is almost negligible as compared to the interaction term, i.e., $\mathcal{R} \approx 0$. As the cloud expands, the interaction energy becomes gradually converted into kinetic energy and this ratio increases until it finally saturates. This shows up in figure 5(b). For a larger disorder, this increase of the ratio saturates more rapidly and the slope of $\mathcal{R}(t)$, which indicates how fast the interaction energy is converted into kinetic energy, decreases. Particularly the lowest plot corresponding to a large disorder shows a rapid saturation of $\mathcal{R}$ due to a strong localization in momentum space. Since the edge of the cloud involves mostly kinetic energy, the behaviour of $\mathcal{R}$ is dominated by the expansion of the central region. When the expansion is stopped by a potential barrier, the corresponding loss in kinetic energy is proportional to the height of the potential barrier. This explains the oscillations of $\mathcal{R}$ that appear in the presence of disorder.

5. Gaussian limit

In this section we study effects of disorder on bosons that are condensed in the ground state of a harmonic oscillator potential. In that case, the solutions of the Gross–Pitaevskii

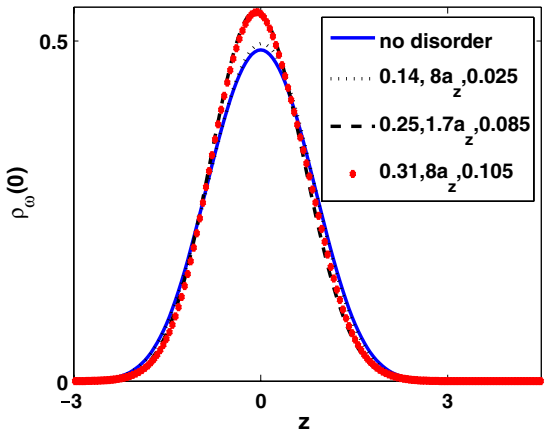

Figure 6. Stationary profile of the condensate density in the presence of disorder. The corresponding values of the average disorder strength $\langle s\rangle$, λ_c and δs are given in the inset.

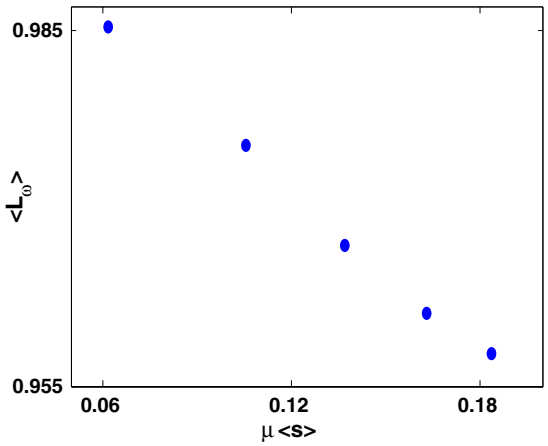

Figure 7. Behaviour of the disorder averaged width $\langle L_\omega\rangle$ of the stationary density profile in the Gaussian limit as a function of the average disorder strength $\mu\langle s\rangle$. The width is normalized by its value in the absence of disorder. For a given value of λ_c, the width is averaged over 200 realizations of the potential. The values of λ_c are those used in figure 2 and, in units of the harmonic oscillator length a_z, they range between $0.55a_z$ (lowest point) and $5a_z$ (highest point). We have used $\mu = 2$ and $2\alpha_{1d} = 0.01$.

equation without disorder are different from those obtained in the Thomas–Fermi limit, and are given by Gaussian profiles centred at the origin.

5.1. Stationary solutions

Like for the Thomas–Fermi regime, stationary solutions of the Gross–Pitaevski equation (16) in the presence of both trapping and disorder are characterized by the average strength $\langle s\rangle$ and the length λ_c. By changing the disorder strength we obtain behaviours such as those displayed in figure 6.

Since interaction effects are negligible in the Gaussian limit, the characteristic length of density variations is set by the harmonic oscillator length a_z, and not by the coherence length ξ as before, the latter being very large in that case. In this regime dominated by confinement, we observe that the shape of the density profile depends weakly on disorder in contrast to the Thomas–Fermi limit, for which this profile follows the variations of the disorder. This is particularly apparent in figures 8(c) and (d), where disorder varies over a length scale smaller than the width of the density profile without leading to fluctuations of this profile.

The density profile is well approximated by a off-centred Gaussian shape,

$$\rho_\omega(z) = A\exp\left(-\frac{(z-z_0)^2}{L_\omega^2}\right), \tag{32}$$

for a large range of disordered potentials (see figure 6(b)). The amplitude A and the width L_ω are related to each other through the normalization. The average width $\langle L_\omega\rangle$ is a decreasing function of the disorder strength $\mu\langle s\rangle$ defined by (17) as represented in figure 7. Thus, the net effect of disorder is to spatially localize the bosons inside a narrower Gaussian.

5.2. Time-dependent solutions

The behaviour of the stationary condensate density profile in the presence of disorder in the Gaussian limit differs from that obtained in the Thomas–Fermi limit. This difference shows up also in the time evolution of the density of the cloud after switching off the trapping potential. The short time expansion of the Thomas–Fermi cloud strongly depends on disorder, whereas in the Gaussian case, it does not. Moreover, in contrast to the Thomas–Fermi case, the zero point motion of the bosons is appreciable. The time evolution of the condensate density after switching off the trap is presented in figure 8 for different strengths of disorder.

We first note that on the same time scale, the density at the centre of the cloud decreases more rapidly than for the Thomas–Fermi case (figure 3). This results from the non-negligible kinetic energy of a Gaussian cloud and the weaker interaction between bosons. Figure 9 displays the time evolution of the average spatial extension $\langle L_\omega\rangle$ of the cloud defined by (28) and the ratio of the average kinetic and interaction energies defined in (31). These two figures outline the difference between Thomas–Fermi and Gaussian time evolutions in the presence of disorder. The spatial extension in figure 9(a) does not show any saturation over comparable time scales, though it grows at a lesser rate with increasing the strength of disorder. Correlatively, the ratio $\mathcal{R}$ in figure 9(b) grows at a much faster rate and it takes a longer time to saturate. We can summarize these observations by saying that though the cloud expansion is indeed prevented by the disorder potential in the Gaussian regime, the suppression is weaker than in the Thomas–Fermi regime and it happens on longer time scales.

6. Soliton solutions for an attractive Bose–Einstein condensate

Having discussed the behaviour of repulsive interacting bosons in the presence of disorder, we now turn to the case of an attractive solitonic condensate in similar situations. As

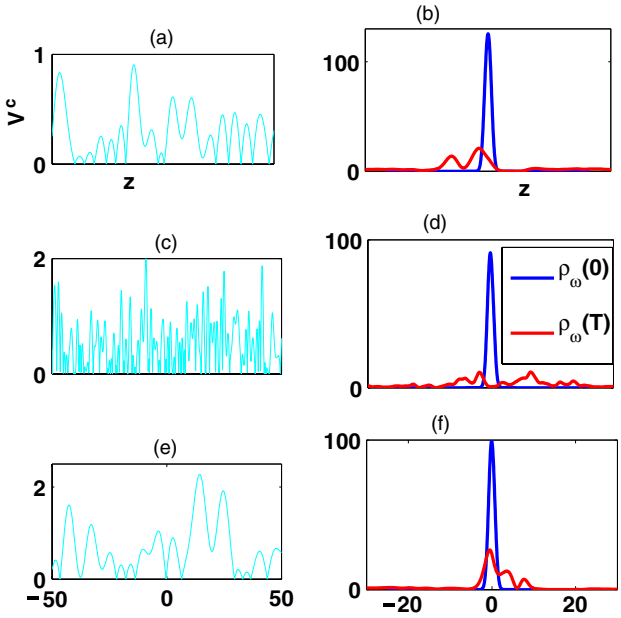

Figure 8. Left (a), (c) and (e) Plot of the disordered potential. The potentials in (a) and (e) vary on the same scale, whereas the potential in (c) varies on a smaller scale. The corresponding values of $\langle s\rangle$, λ_c and δs are respectively (0.14, $8a_z$, 0.025), (0.25, $1.66a_z$, 0.0846) and (0.31, $8a_z$, 0.105). Right (b), (d) and (f) time evolution of the density corresponding to the potentials plotted on the left. The initial stationary value of the density is denoted by $\rho_\omega(0)$ and $\rho_\omega(T)$ is computed at the time $T = 25/\omega_z$. We have used $\mu = 2$ and $2\alpha_{1d} = 0.01$.

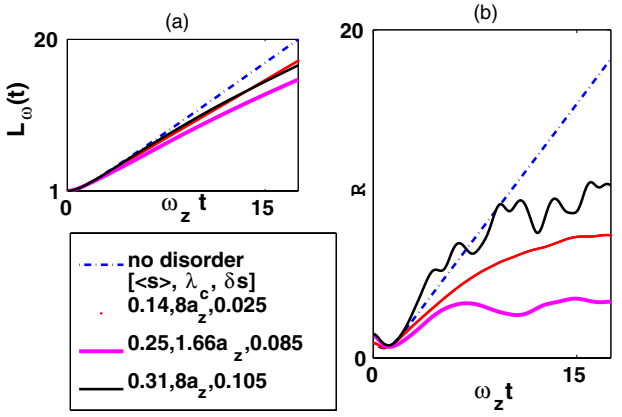

Figure 9. (a) Time evolution of the spatial extension $L_\omega(t)$ of the cloud for disorders of different strengths V_m and length scales of variation λ_c. The disordered potentials are those used in figure 8 and the corresponding parameters are indicated ($\langle s\rangle$, λ_c, δs) in the inset. $L_\omega(t)$ is expressed in units of its value at $t = 0$. (b) Corresponding time evolution of the ratio $\mathcal{R}$ is defined in (31).

we shall see, the change of the nature of the interaction modifies the behaviour of the soliton solution with disorder as compared to the previous cases of Thomas–Fermi and Gaussian condensates. In contrast to equation (6) describing a repulsive interaction, equation (11) involves one free parameter only ($\alpha_{1d} = -1$). As we have already mentioned, a change in α_{1d} only redefines the width of the soliton

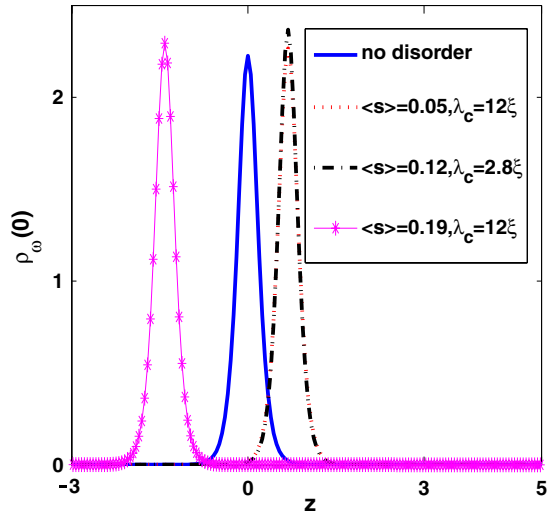

Figure 10. Stationary density profile of a bright soliton in the presence of disorder. The chemical potential is $\mu = -20$ and $\alpha_{1d} = -1$. The disordered potential is characterized by $|s|$ (since $\mu < 0$) and λ_c. $\langle s\rangle$ is the average of $|s|$.

proportional to $1/\sqrt{\mu}$. In what follows, the width is always kept less than ξ.

6.1. *Stationary profiles*

We start with the study of the stationary solutions of equation (11) with the addition of a random potential, namely,

$$-\mu\phi(z) + \partial_z^2\phi(z) + V_d\phi(z) + 2|\phi|^2\phi = 0. \qquad (33)$$

It is important to note that, in contrast to previous cases, there is no trapping potential, so that in the absence of disorder, the solution is translational invariant. Numerically, we start with a randomly chosen initial guess which, once iterated, gives a solution located around the initial trial function. The overall shape of the stationary solution turns out to be independent of disorder, meaning that this shape can still be fitted with a function of the type $A_s\mathrm{sech}(B_s(z - z_0))$, where A_s and $B_s = 1/L_\omega$ are respectively the amplitude and the inverse width of the soliton. This feature appears clearly in figure 10 where the profile of the bright soliton has been plotted for several realizations of the potential. But, both the width and the amplitude depend on disorder as shown in figure 11 which displays the behaviour of the width for an increasing strength of disorder. We have also checked the dependence upon length scales λ_c. Those features look similar to those obtained in the Gaussian limit. But they are essentially different. Whereas the soliton profile results from the comparison between kinetic and negative interaction energies, the Gaussian profile is obtained from the comparison between kinetic and confinement energies. This difference will manifest itself in the time evolution of the solitonic condensate.

6.2. *Time-dependent solutions*

We now study the time evolution of the stationary solutions obtained previously, and not initial solutions given by (10)

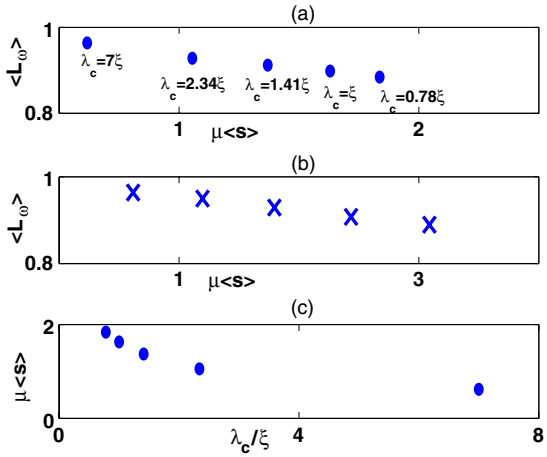

Figure 11. Disorder averaged width $\langle L_\omega \rangle$ of the stationary profile of a soliton as a function of the strength of disorder. (a) Here (*), λ_c is lowered which corresponds to stronger fluctuations of the disorder, while V_m is kept fixed. (b) Here ($\times$), the strength V_m of the disordered potential is increased keeping fixed the spatial scale of variation λ_c. $\langle L_\omega \rangle$ is expressed in units of its value in the absence of disorder and, for each case, it is averaged over 200 realizations of the potential. The average potential is characterized by $|s|$ since $\mu < 0$. The values of λ_c are indicated in the figure. We have taken $\mu = -20$ and $2\alpha_{1d} = -1$. (c) The plot showing the change of $\mu\langle s \rangle$ as the cut-off λ_c changes for the values used in part (a).

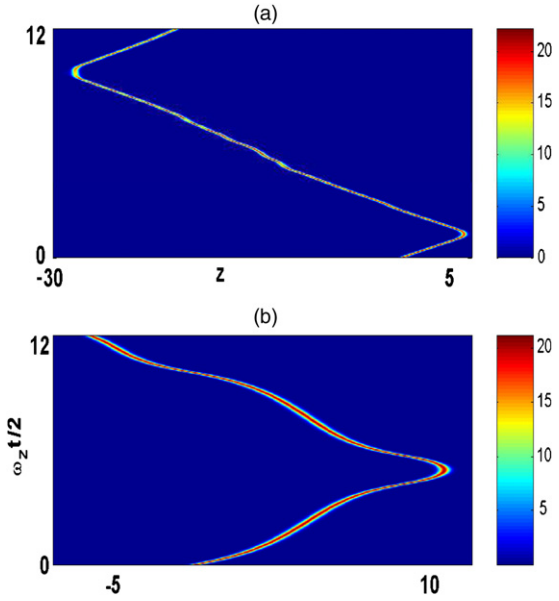

Figure 12. Time evolution of a boosted soliton in the presence of disorder. The chemical potential is $\mu = -20$, the dimensionless velocity at $t = 0$ is $V_s = 5$ and $\alpha_{1d} = -1$. The disorder potential is characterized by $|s|$ (since $\mu < 0$) and λ_c. (a) Fastly varying disorder with $\langle s \rangle = 0.12$, $\delta s = 0.162$ and $\lambda_c = 2.8\xi$. (b) Stronger but slowly varying disorder with $\langle s \rangle = 0.19$, $\delta s = 0.372$ and $\lambda_c = 12\xi$.

unlike the case considered in [16]. For this purpose, we first boost the soliton by giving it a finite (dimensionless) velocity $V_s = 5$. In the absence of disorder, the soliton travels a distance $z = V_s t$ over a time t without any change in its density profile. In the presence of a weak and smooth enough disorder, we observe that the soliton propagates retaining its initial ($t = 0$) shape, over distances comparable to the non-disordered case. A weak disorder potential has thus a negligible effect on the soliton motion. For a stronger disorder strength (i.e., for a smaller value of λ_c and a larger value of $\langle s \rangle$), the time behaviour is displayed in figures 12(a) and (b). In both cases, the soliton behaves classically and it becomes spatially localized, i.e. that it bounces back from high potential barriers typically higher than the kinetic energy. However, we do not observe a significant change in the shape of the soliton. Its width fluctuates as the soliton travels through the disordered potential and bounces back and forth. When the strength of disorder is higher, the soliton motion is clearly not linear (figure 12(b)). This kind of motion can be qualitatively explained by considering the soliton as a massive classical particle of mass mN, where m and N are respectively the mass and the number of atoms in the condensate. Deviations from the linear motion result from the spatially varying force exerted on the soliton by the disorder potential. This kind of description is valid as long as the disorder potential remains smooth over the width of the soliton. Similar behaviours have been discussed in the context of soliton chaos in spatially periodic potentials [54], although the physical origin is different from the case discussed here. At the present stage of experiment [38], such a behaviour could be verified by studying the time evolution of a bright soliton in an optical speckle pattern.

7. Conclusion

We have performed a detailed numerical investigation of stationary solutions and time evolution of one-dimensional Bose–Einstein condensates in the presence of a random potential. Stationary solutions which correspond either to the attractive interaction bright soliton or to repulsive interaction Gaussian matter waves with repulsive interactions in the regime where confinement dominates, behave in a qualitatively similar way. In contrast, the stationary solutions that correspond to a repulsive interacting Thomas–Fermi condensate depend strongly on the strength of disorder and on its spatial scale of variations.

The time evolution of stationary solutions depends also significantly on the regime we consider. Although transport gets inhibited both for the attractive and repulsive interaction, this occurs in a very different way. For the repulsive case the centre and the edge of the cloud behave differently and both are ultimately localized in a deep enough potential well. In the interaction dominated Thomas–Fermi regime, the main part of the cloud remains localized and edges that correspond to low densities and correlatively weaker interactions, propagate further away. A study of the corresponding momentum distribution of the cloud indicates a stronger localization of the matter wave in low momentum states for an increasing strength of the disorder potential. On the other hand, a moving bright soliton behaves very much like a single particle and it bounces back from a steep potential with its motion reversed. This behaviour of a bright soliton may be contrasted against the behaviour of a dark soliton in the presence of disorder which has been investigated recently [28].

For the values of the disorder strength and the nonlinearity we have considered, we observe a behaviour of solutions of the Gross–Pitaevskii equation that are mostly driven by the nonlinearity, i.e., by interactions. Disorder plays mostly the role of a landscape within which a classical solution evolves in time. We did not observe, for the relatively large range of disorder and interaction parameters we have considered, a behaviour close to Anderson localization, namely where spatially localized solutions result from interference effects. Since disorder is expected to be stronger in one-dimensional systems, we may conclude that, for the currently accessible experimental situations, Anderson localization effects will not be observable [18, 22, 33] due to the strength of the interaction term. Alternative setups are thus required in order to observe quantum localization of matter waves, having weak or zero interaction (e.g., by monitoring Feschbach resonances [26]).

The signature of Anderson localization in the nonlinear transport of a BEC in a wave-guide geometry has been studied in [31]. There, the transmission coefficient has been shown to be exponentially decreasing with the system size below a critical interaction strength. But the different types of disorder and the matter wave density at $t = 0$ make a direct comparison with these results difficult.

Acknowledgments

SG thanks Hrvoje Buljan for his help in numerical computation. He also thanks the Technion and Okayama University for generous support. This research is supported in part by the Israel Academy of Sciences and by the Fund for Promotion of Research at the Technion.

References

[1] Anderson P W 1958 *Phys. Rev.* **109** 1492
[2] Belzons M, Guazzelli E and Parodi O 1988 *J. Fluid Mech.* **186** 539
Belzons M, Devillard P, Dunlop F, Guazzelli E, Parodi O and Souillard B 1987 *Europhys. Lett.* **4** 909
[3] Dépollier C, Kergomard J and Laloë F 1986 *Ann. Phys. (France)* **11** 457
[4] Akkermans E and Maynard R 1984 *J. Physique (France)* **45** 1549
[5] Abrahams E, Anderson P W, Licciardello D C and Ramakrishnan T V 1979 *Phys. Rev. Lett.* **42** 673
[6] Schwartz T, Bartal G, Fishman S and Segev M 2007 *Nature* **446** 52
[7] Chabanov A A, Stoytchev M and Genack A Z 2000 *Nature* **404** 850
[8] Wiersma D S, Bartolini P, Lagendijk A and Righini R 1997 *Nature* **390** 671
[9] Scheffold F, Lenke R, Tweer R and Maret G 1999 *Nature* **398** 207
Storzer M *et al* 2006 *Phys. Rev. Lett.* **96** 063904
[10] Kramer B and MacKinnon A 1993 *Rep. Prog. Phys.* **56** 1469
[11] Lee P A and Ramakrishnan T V 1985 *Rev. Mod. Phys.* **57** 287
[12] Akkermans E and Montambaux G 2007 *Mesoscopic Physics of Electrons and Photons* (Cambridge: Cambridge University Press)
[13] Akkermans E and Montambaux G 2004 *J. Opt. Soc. Am.* B **21** 101
[14] Devillard P and Souillard B 1986 *J. Stat. Phys.* **43** 423
[15] Doucot B and Rammal R 1987 *Eur. Phys. Lett.* **3** 969
Doucot B and Rammal R 1987 *J. Phys. (Paris)* **48** 527
[16] Kivshar Y S, Gredeskul S A, Sanchez A and Vazquez L 1990 *Phys. Rev. Lett.* **64** 1693
[17] Lye J E, Fallani L, Modugno M, Wiersma D, Fort C and Inguscio M 2005 *Phys. Rev. Lett.* **95** 070401
[18] Fort C, Fallani L, Guarrera V, Lye J, Modugno M, Wiersma D S and Inguscio M 2005 *Phys. Rev. Lett.* **95** 170410
[19] Kruger P, Andersson L M, Wildermuth S, Hofferberth S, Haller E, Aigner S, Groth S, Bar-Joseph I and Schmiedmayer J 2005 arXiv cond-mat/0504686
[20] Clément D, Varón A F, Hugbart M, Retter J, Bouyer P, Sanchez-Palencia L, Gangardt D M, Shlyapnikov G V and Aspect A 2005 *Phys. Rev. Lett.* **95** 170409
[21] Clement D, Varon A F, Retter J A, Sanchez-Palencia L, Aspect A and Bouyer P 2006 *New J. Phys.* **8** 165
[22] Schulte T, Drenkelforth S, Kruse J, Ertmer W, Arlt J, Sacha K, Zakrzewski J and Lewenstein M 2005 *Phys. Rev. Lett.* **95** 170411
[23] Damski B, Zakrzewski J, Santos L, Zoller P and Lewenstein M 2003 *Phys. Rev. Lett.* **91** 080403
Pugatch R, Bar-Gil N, Katz N, Rowen E and Davidson N 2006 arXiv cond-mat/0603571
[24] Sanpera A *et al* 2004 *Phys. Rev. Lett.* **93** 040401
[25] Wang D W, Lukin M D and Demler E 2004 *Phys. Rev. Lett.* **92** 076802
[26] Gavish U and Castin Y 2005 *Phys. Rev. Lett.* **95** 020401
[27] Paredes B, Verstraete F and Cirac J I 2005 *Phys. Rev. Lett.* **95** 140501
[28] Bilas N and Pavloff N 2005 *Phys. Rev. Lett.* **95** 130403
[29] Fallani L, Lye J, Guarrera V, Fort C and Inguscio M 2006 arXiv cond-mat/0603655
[30] Modugno M 2006 *Phys. Rev.* A **73** 013606
[31] Paul T, Leboeuf P, Pavloff N, Richter K and Schdagheck P 2005 *Phys. Rev.* A **72** 063621
[32] Gimperlein H, Wessel S, Schmiedmayer J and Santos L 2005 *Phys. Rev. Lett.* **95** 170401
[33] Singh K G and Rokshar D S 1994 *Phys. Rev.* B **49** 9013
[34] Olshanii M 1998 *Phys. Rev. Lett.* **81** 938
[35] Pitaevskii L and Stringari S 2003 *Bose–Einstein Condensation* (Oxford: Oxford University Press)
[36] Petrov D S, Shlyapnikov G V and Walraven J T M 2000 *Phys. Rev. Lett.* **85** 3745
Petrov D M, Gangardt D M and Shlyapnikov G V 2004 *J. Phys. IV France* **116** 3
[37] Tonks L 1967 *Phys. Rev.* **50** 955
Girardeau M D 1960 *J. Math. Phys.* **1** 516
Yang C N and Yang C P 1969 *J. Math. Phys.* **10** 1115
[38] Khaykovich L, Schreck F, Ferrari G, Bourdel T, Cubizolles J, Carr L D, Castin Y and Salomon C 2002 *Science* **296** 1290
Strecker K E, Partridge G B, Truscott A G and Hulet R G 2002 *Nature* **417** 150
Eiermann B, Anker Th, Albiez M, Taglieber M, Treutlein P, Marzlin K P and Oberthaler M K 2004 *Phys. Rev. Lett.* **92** 230401
[39] Carr L D and Castin Y 2002 *Phys. Rev.* A **66** 063602
[40] Sulem C and Sulem P L 1999 *The Nonlinear Schrödinger Equation Self-Focusing and Wave Collapse* (New York: Springer)
[41] Huntley J M 1989 *Appl. Opt.* **28** 4316
[42] Petviashvili V I 1976 *Sov. Plasma Phys.* **2** 257
[43] Ablowitz M J and Musslimani Z H 2003 *Physica* D **184** 276
[44] Musslimani Z H and Yang J 2004 *J. Opt. Soc. Am.* B **21** 973
[45] Ablowitz M J and Musslimani Z M 2005 *Opt. Lett.* **30** 2140
[46] Bao W, Jaksch D and Markowich P A 2003 *J. Comput. Phys.* **187** 318

[47] Sanchez-Palencia L 2006 *Phys. Rev.* A **74** 053625
[48] Lugan P, Clement D, Bouyer P, Aspect A, Lewenstein M and Sanchez-Palencia L 2007 *Phys. Rev. Lett.* **98** 170403
[49] Sanchez-Palencia L *et al* 2007 *Phys. Rev. Lett.* **98** 210401
[50] Richard S, Gerbier F, Thywissen J H, Hugbart M, Bouyer P and Aspect A 2003 *Phys. Rev. Lett.* **91** 010405
[51] Shapiro B 2007 *Phys. Rev. Lett.* **99** 060602
[52] Chen Y P, Hitchcock J, Dries D, Junker M, Welford C and Hulet R G 2007 arXiv: 0710.5187
[53] Bilas Nicolas and Pavloff Nicolas 2006 *Eur. Phys. J.* D **40** 387
Lugan P, Clement D, Bouyer P, Aspect A and Sanchez-Palencia L 2007 *Phys. Rev. Lett.* **99** 180402
[54] Scharf R and Bishop A R 1992 *Phys. Rev.* A **46** R2973
Martin A D, Adams C S and Gardinar S A 2007 *Phys. Rev. Lett.* **98** 020402